HHS Public Access

Author manuscript

Biochemistry. Author manuscript; available in PMC 2016 October 06.

Published in final edited form as:

Biochemistry. 2015 October 6; 54(39): 6071–6081. doi:10.1021/acs.biochem.5b00659.

Binuclear CuA Formation in Biosynthetic Models of Cu_A in Azurin Proceeds via a Novel $Cu(Cys)_2His$ Mononuclear Copper Intermediate

Saumen Chakraborty[†,§], **Michael J. Polen**[†,±], **Kelly N. Chacón**[‡,⊥], **Tiffany D. Wilson**[†], **Yang Yu**[†,≠], **Julian Reed**[†], **Mark J. Nilges**[†], **Ninian J. Blackburn**[‡,*], and **Yi Lu**[†,*]

[†]Department of Chemistry, University of Illinois at Urbana-Champaign, Urbana, IL 61801, USA

[‡]Institute of Environmental Health, Oregon Health & Sciences University, Portland, OR 97239, USA

Abstract

Cu_A is a binuclear electron transfer (ET) center found in cytochrome *c* oxidases (C*c*Os), nitrous oxide reductases (N_2ORs), and nitric oxide reductase (NOR). In these proteins, the Cu_A centers facilitate efficient ET ($k_{ET} > 10^4\ s^{-1}$) under low thermodynamic driving forces (10–90 mV). While the structure and functional properties of Cu_A are well understood, a detailed mechanism of copper incorporation into the protein and the identity of the intermediates formed during the Cu_A maturation process are still lacking. Previous studies of the Cu_A assembly mechanism *in vitro* using a biosynthetic model Cu_A center in azurin (Cu_AAz) identified a novel intermediate X (I_x) during reconstitution of the binuclear site. However, due to the instability of I_x and the coexistence of other Cu centers, such as Cu_A' and type 1 copper centers, the identity of this intermediate could not be established. Here, we report the mechanism of Cu_A assembly using variants of Glu114XCu_AAz (X=Gly, Ala, Leu, Gln), the backbone carbonyl of which acts as a ligand to the Cu_A site, with a major focus on characterization of the novel intermediate I_x. We show that Cu_A assembly in these variants proceeds through several types of Cu centers, such as mononuclear red type 2 Cu, the novel intermediate I_x, and blue type 1 Cu. Our results show that the backbone flexibility of the Glu114 residue is an important factor in determining the rates of T2Cu→I_x formation, suggesting that the Cu_A formation is facilitated by swinging of the ligand loop, which internalizes the T2Cu capture complex to the protein interior. The kinetic data further suggests that the nature of the Glu114 side chain influences the timescales on which these intermediates are formed, the wavelengths of the absorption peaks, and how cleanly one intermediate is converted to another. Through careful understanding of these mechanism and optimization of the conditions,

[*]Corresponding authors: ; Email: yi-lu@illinois.edu; ; Email: blackbni@ohsu.edu
[§]Center for Integrated Nanotechnologies, Los Alamos National Laboratory, Los Alamos, NM 87545, USA
[±]Department of Chemistry, Carnegie Mellon University, Pittsburgh, PA 15213, USA
[⊥]Department of Chemistry, Reed College, Portland OR 97202, USA
[≠]University of Chinese Academy of Sciences, Beijing 100049, P. R. China

The authors declare no competing financial interest.

Supporting Information:
Stopped flow data of Glu114XCu_AAz variants under O_2-rich and anaerobic conditions, full EPR parameters of all intermediates, Specfit derived spectra of intermediates, EPR and EXAFS data of holo Glu114XCu_AAz variants, and spin quantification of Glu114GlyCu_AAz. This material is available free of charge via the Internet at http://pubs.acs.org.

we have obtained I_x in ~80–85% population in these variants, which allowed us to employ UV-Vis, EPR, and EXAFS spectroscopic techniques to identify the I_x as a mononuclear $Cu(Cys)_2(His)$ complex. Since some of the intermediates have been proposed to be involved in the assembly of native Cu_A, these results shed light on the structural features of the important intermediates and mechanism of Cu_A formation.

Graphical abstract

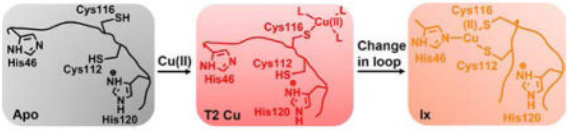

Introduction

Electron transfer (ET) is essential for many biological processes, such as photosynthesis, respiration, and dinitrogen fixation.[1] To facilitate these processes, copper proteins involved in redox and ET process, called cupredoxins, are often utilized, and they share a common Greek-key-β-barrel fold, where the majority of copper-coordinating ligands occur in a loop.[2–9] A Cys thiolate is a ligand common in cupredoxins, which makes these proteins intense in color, due to $S_{Cys}\rightarrow Cu$ charge transfer (CT) transitions. Three types of copper sites are typically found in cupredoxins: the blue mononuclear type 1 copper (T1Cu) with distorted trigonal geometry, the red mononuclear type 2 copper (T2Cu) with square pyramidal geometry, and the purple binuclear Cu_A with a diamond core geometry.[3, 10–12] While the T1Cu and Cu_A sites facilitate ET, the T2Cu sites are generally involved in catalysis.[10]

One important class of these copper sites is the binuclear purple Cu_A, which is found in enzymes involved in aerobic and anaerobic respiration, such as cytochrome *c* oxidases (C*c*Os),[13–15] quinol oxidase (SoxH),[16, 17] nitrous oxide reductases (N_2ORs),[18, 19] and nitric oxide reductase (qCu_ANOR).[20] In these proteins, the Cu_A site acts as a terminal ET center by accepting electrons from donors, such as cytochromes *c,* and transferring them to redox partners with high efficiency (e.g. ET rate, $k_{ET} > 10^4\ s^{-1}$), despite low thermodynamic driving forces (10–90 mV) for such ET. The Cu_A centers are characterized by a mixed valence $[Cu^{(+1.5)}\text{-}Cu^{(+1.5)}]$ site, containing a weak Cu-Cu bond, in which one electron is delocalized between the two copper ions.[21–23] The two copper ions are coordinated by two Cys residues to form a rigid “diamond” core, and each metal ion is also coordinated by a His residue (Fig. 1A). These structural features of the Cu_A site also bestow them with unique spectroscopic signatures. The UV-vis of Cu_A sites have two $S_{Cys}\rightarrow Cu(II)$ CT at ~480 and 530 nm (ε ~3000–4000 $M^{-1}cm^{-1}$), and a broad peak due to a Cu-based ($\psi\rightarrow\psi^*$) transition centered at ~800 nm (ε ~2000 $M^{-1}cm^{-1}$), giving the Cu_A a strong purple color.[16, 21, 24–27] The electron paramagnetic resonance (EPR) spectrum consists of a seven line hyperfine splitting pattern due to valence delocalization of the unpaired d electron between the two Cu nuclei, each having a nuclear spin I = 3/2.[22] On the other hand, the T1Cu center also displays intense blue color, due to strong absorbance at ~600 nm (ε ~2000–6000 $M^{-1}cm^{-1}$) that arises from $S_{Cys}(\pi)\rightarrow Cu(II)$ CT transition. It also differs from the typical T2 Cu center

by a small 4-line EPR hyperfine splitting pattern, which is due to valence delocalization of the unpaired d electron onto the mononuclear Cu. In general, the Cu_A center displays even smaller hyperfine splitting (A_z ~30–40 x 10^{-4} cm^{-1}) than T1Cu site (A_z ~30–90 x 10^{-4} cm^{-1}) as the hyperfine splitting is divided into two copper atoms.[10] The red T2Cu center, in contrast, exhibits an intense absorption ~360–400 nm, due to a $S_{Cys(\sigma)}\rightarrow Cu(II)$ CT transition. It also displays 4-line EPR hyperfine splitting pattern with a much larger hyperfine splitting (A_z ~130–180 x 10^{-4} cm^{-1}) than those in Cu_A or T1Cu centers, reflecting a lesser extent of covalency.[28, 29] From phylogenetic and sequence analyses, it has been suggested that the blue T1Cu, red T2Cu, and purple Cu_A sites have evolved from a common ancestor.[30] All three types of Cu centers were observed in a study involving *in vitro* reconstitution of the Cu_A site of N_2OR from *Paracoccus denitrificans.*[31]

Due to the presence of multiple cofactors in the proteins containing Cu_A centers (hemes in C*c*Os and qCu_ANOR, tetranuclear Cu_Z in N_2ORs), studying the Cu_A sites in these proteins has been hindered by intense and overlapping spectral features.[16, 17, 19, 20] One strategy that has been employed to study Cu_A sites involves expressing the soluble Cu_A domain from C*c*O and reconstituting the Cu_A site *in vitro.*[16, 25–27, 32–36] In a second strategy the Cu_A ligands have been engineered in another cupredoxin protein followed by *in vitro* reconstitution of the binuclear site.[37–40] By replacing the Cu binding loop from T1Cu proteins with the Cu_A loop from C*c*O, the Cu_A site was successfully engineered into CyoA domain of a copper-less quinol oxidase (called Cu_A-CyoA) and blue T1Cu proteins amicyanin (called Cu_AAmi) and azurin (Az, called Cu_AAz).[38,37, 40–44]

While the Cu_A center has been well studied, one of the remaining challenges in understanding this class of copper center is the mechanism of its formation, particularly how the mixed valence species [$Cu^{(+1.5)}$-$Cu^{(+1.5)}$] is formed from either Cu(I) or Cu(II) ions. The red T2Cu Sco1 protein from the inner mitochondrial membrane, which exhibits $Cu(Cys)_2$His ligation, has been implicated to be the chaperone responsible for Cu delivery to the Cu_A site.[45–50] Quite interestingly, binding of both Cu(II) and Cu(I) to Sco1 has been proposed to be important for normal functioning of this protein.[51–53] Alternatively, it has been proposed that Sco1 acts as disulfide reductase to keep the active site Cys of Cu_A in the reduced state or to maintain a proper redox buffering of metal ions. The latter inference stems from the fact that Sco1 possesses the thioredoxin fold.[50, 54, 55] In *Bacillus subtilis,* another protein, YpmQ, which is the yeast homologue of Sco1, and has a $Cu(Cys)_2$His ligation, has also been proposed to be required for Cu_A assembly. Furthermore, the periplasmic protein PCu_AC, found in several prokaryotes has been shown to deliver Cu(I) to apo Cu_A, forming the binuclear Cu(I)-Cu_A site.[54]

In order to gain insight into Cu_A assembly, studies have been undertaken using both soluble domain of *Thermus thermophilus (Tt)* Cu_A[56, 57] and biosynthetic models of Cu_A in azurin (called Cu_AAz).[58, 59] A single intermediate was observed as a rapidly-formed green Cu center in the soluble domain of *Tt* Cu_A and this intermediate was identified as a mononuclear $Cu(II)(Cys)_2(His)$ complex, based on UV-vis, EPR and X-ray absorption spectroscopy (XAS) studies.[56] On the other hand, addition of 10-fold excess $CuSO_4$ to the apo Cu_AAz, a red T2Cu intermediate was formed within 10 ms, followed by formation of the purple Cu_A site at longer times.[58] Recently, it has been shown that under sub-equivalent

Cu(II) addition, the formation of binuclear Cu_A center is an intricate process, such that in addition to the formation of the red T2Cu intermediate, a novel green copper intermediate, I_x, and a blue T1Cu intermediate was observed prior to Cu_A formation.[59] The proposed mechanism invoked the formation of an initial red T2Cu involving Cys116 that is close to the protein exterior. The next step of the kinetic process is then branched into a) the formation of binuclear Cu_A', a Cu_A lacking His120 ligation, and b) a conformational change of the metal binding loop, leading to reorientation of the capture complex toward the protein interior and accompanying ligation by Cys112 and His46, forming I_x. Through comparison to the spectral properties of Cu(II)-substituted horse liver alcohol dehydrogenase (HLADH),[60–62] a Cu(II)-dithiolate complex was proposed as the identity of I_x. However, the exact ligand environment of I_x could not be established, as it was a short-lived intermediate present in a mixture with other species. The next step of the mechanism proposed the formation of a T1Cu complex from oxidation of the reduced Cu(I) product of I_x. The T1Cu complex was finally converted to the valence-delocalized Cu_A site via incorporation of *in situ* reduced Cu(I).

While the above results are valuable, they do not fully clarify the mechanism of the Cu_A formation. A critical missing piece of this mechanistic puzzle is the identity of the I_x intermediate. To identify this I_x, we examine the X-ray structure of Cu_AAz, which reveals that the side chain of Glu114, whose backbone carbonyl is very close to one of the Cu ions (2.2 Å), is positioned in between two hydrophobic amino acids, Leu86 and Tyr72 (Fig. 1A).[63] We thus hypothesize that the Glu114 side chain is likely more solvent exposed in the apo form due to the negative charge on the Glu carboxylate at neutral pH. In the holo form, the coordination of the backbone carbonyl group of Glu114 to one of the copper ions likely requires a specific orientation of the Glu114 side chain in between the two hydrophobic amino acids. As a result of this steric effect, the helices housing these two amino acids are pushed away from each other (Fig. 1B, purple). Interestingly, no such steric repulsion of the helices in blue T1Cu Az is observed (Fig. 1B, blue). In contrast, the corresponding Glu side chain, found in the majority (80%) of native C*c*Os is oriented towards the membrane interior, where it is coordinated to a Mg(II) ion.[14]

Herein, we investigate the effect of the Glu114 side chain on the sterics of the Cu binding loop and on the Cu_A assembly, by systematic substitution of this side chain with other side chains such as Gly (lacking a side chain), Ala (having a smaller, more hydrophobic methyl group), Leu (same chain length but more hydrophobic), and Gln (same chain length, but with no charge). Thus, the Gly, Ala, and Leu mutations would allow us to test the effect of increasing side chain bulk, while the Leu and Gln mutations should address the role of side chain polarity on the mechanism of the Cu_A formation. The specific issues we try to address in this report are: a) whether these mutations have any effect on the overall mechanism of Cu_A formation, in particular the rate of the T2Cu→I_x step of the mechanism, as this step was proposed to involve a conformational change in the metal binding loop, and b) whether these mutations affect the formation and decay kinetics of these intermediates. Of particular interest was to obtain the I_x in higher purity compared to the original Cu_AAz and determine its identity.

Materials and Methods

Protein Expression and Purification

Plasmids of the Cu_AAz variants Glu114Gly/Ala/Leu/Gln containing a periplasmic leader sequence from *Pseudomonas aeruginosa* were cloned into pET-9a vector and expressed in *E.coli* BL21*(DE3) (Invitrogen) competent cells. Expression and purification was done as described previously,[38, 44, 58, 59] with some modifications. Bacterial cultures were grown in 2XYT media at 25°C until an OD of ~0.6–1.0 was reached. Protein expression was induced with Isopropyl β-D-1-thiogalactopyranoside (IPTG) (~200mg/2L) and allowed to grow for 4 hours. Cells were harvested and re-suspended in 20% sucrose, 1 mM Ethylenediaminetetraacetic acid (EDTA), 30 mM 2-Amino-2-hydroxymethyl-propane-1,3-diol (Tris).HCl solution. After centrifugation the periplasmic membranes were lysed by osmotic shock solution containing 4 mM NaCl and 1 mM Dithiothreitol (DTT). Following centrifugation, the supernatant was treated with 500 mM NaOAc pH 4.1 to precipitate the impurities. The solution was centrifuged one final time and the supernatant was applied to SP Sepharose cation exchange column (GE Healthcare) pre-equilibrated with 50 mM NH_4OAc pH 4.1, and the protein was eluted using a shallow gradient of 50 mM NH_4OAc pH 6.35. The fractions containing the apo protein were pooled, pH adjusted to 6.3 and further purified by HiTrap Q-Sepharose anion exchange column (GE Healthcare). The colorless apo protein was then concentrated to ~10 mL and further subjected to a size exclusion column (Sephacryl S100, GE Healthcare) to separate misfolded protein. 50 mM NH_4OAc pH 6.35 was used as the elution buffer. The purity and the identity of the properly folded apo protein were verified by electrospray ionization mass spectrometry. Aliquots of apo proteins were flash frozen and stored at −80°C until further use. Whenever required, the apo protein was thawed, exchanged into Universal Buffer (UB) containing 40 mM 2-(*N*-morpholino)ethanesulfonic acid (MES), 3-(N-morpholino)propanesulfonic acid (MOPS), Tris, and, N-cyclohexyl-2-hydroxyl-3-aminopropanesulfonic acid (CAPS), 50 mM NaOAc, and 100 mM $NaNO_3$ at the appropriate pH using Sephadex G-25 desalting columns and concentrated to the required concentration using Amicon Ultra filtration membranes (Millipore). Protein concentrations were determined using $\varepsilon_{280} = 8440\ M^{-1}cm^{-1}$.

Stopped flow UV-vis Absorption Spectroscopy

Stopped flow UV-Vis absorbance data were collected on an Applied Photophysics Ltd. (Leatherhead, U.K.) SX18.MV stopped flow spectrophotometer equipped with a 256 element photodiode array detector. Equal volumes of 0.5 mM apo protein in UB pH 7 (UB 7) and 0.2 mM $CuSO_4$ solutions (1.0 : 0.4 eq. protein : $CuSO_4$ ratio) were mixed by two syringes and spectra were collected over 1000 s on logarithmic scale containing 200 data points with 1 ms sampling time. The final concentrations of protein and $CuSO_4$ were 0.25 mM and 0.1 mM, respectively. A water bath connected to the instrument was used to maintain the temperature at 15°C. For anaerobic stopped-flow experiments the protein and the buffer were degassed on a Schlenk line by three freeze-pump-thaw cycles. Prior to mixing, the stopped-flow instrument was washed with degassed buffer. Similarly, for O_2-rich experiments, the buffer was made O_2-saturated by purging with O_2 for ~15 minutes prior to the experiments. Raw data were subjected to global analysis using SpecFit/32 (Spectrum Software Associates, Inc.).

Global Fit Analysis of the Stopped flow Data

The raw stopped-flow data were processed using SpecFit/32 in order to deconvolute the complex spectral features and multiple kinetic processes. The data analysis is based on Single Value Decomposition (SVD) and non-linear least square fits of the experimental data in an iterative process. During the fitting process a set of kinetic models that seem most consistent with the experimental data were input into the software and fit globally. Using the information from the initial fitting process, the kinetic models were modified accordingly until satisfactory fit results were obtained based on statistics and kinetic parameters.

Kinetic UV-vis Absorption Spectroscopy

Kinetic UV-vis absorption data of samples containing 0.25 mM apo protein in UB 7 and 0.1 mM $CuSO_4$ were collected with constant stirring at 10°C on an Agilent 8453 photodiode array spectrophotometer connected with a water bath cooling system. A lower temperature (10°C) was chosen in the kinetic UV-vis absorption experiment than that (15°C) in the stopped-flow UV-Vis absorption experiment, because of concerns of potential stability issue of the proteins at much longer time scale in the kinetic UV-vis absorption experiment than that in the stopped-flow experiment. Because of this temperature difference, the kinetic rate constants (see Table 1) were obtained only from the stopped-flow data. For these experiments, 1000 °L of 0.5 mM apo protein in UB 7 was taken on a 1cm x 1cm cuvette with stirring and the instrument was set to collect data for 3600 s with scan time of 0.5 s incremented by 5% after 30 s to reduce the number of data points. After collecting a few spectra, 1000 μL of 0.2 mM $CuSO_4$ was added to the apo protein and the cap of the cuvette was sealed with parafilm. The final concentrations of protein and $CuSO_4$ were 0.25 mM and 0.1 mM. After 3600 s, another experiment was started to continue for additional 10–24 hours using a longer scan time of 600 s as the later kinetic processes were slow. In other instances, similar experiments were performed with solutions containing equal volume of 3 mM apo protein in UB 7 and 1.2 mM $CuSO_4$, amounting to a final concentration of 1.5 mM apo protein and 0.6 mM $CuSO_4$. These experiments were performed at the concentrations similar to those of target EPR experiments, so as to determine the time points at which different intermediates formed with maximum population in order to characterize them by EPR. Due to fast formation and decay of the red T2 Cu intermediate (~100 ms), we focused on characterizing the later intermediates, in particular I_x, as this intermediate was not thoroughly characterized previously. From inspection of the UV-vis absorbance data from these experiments, I_x formed with maximum population at ~50–60 s.

Electron Paramagnetic Resonance Spectroscopy

EPR data were collected using an X-band Varian E-122 spectrometer at the Illinois EPR Research Center (IERC) at 30 K using liquid He and an Air Products Helitran cryostat. Magnetic fields were calibrated with a Varian NMR Gaussmeter while the microwave frequencies were measured with an EIP frequency counter. Based on the results of the kinetic UV-vis experiments, EPR samples were flash frozen in liquid N_2 with 22% glycerol as glassing agent at a broad range of time points after $CuSO_4$ addition. The time points were chosen so as to obtain as much information as possible about the discrete kinetic processes and the species present therein at that time point. The earliest time points were determined to

capture the I_x in each mutant. The earliest time point (50s-60s) samples were prepared by quick mixing of equal volumes of 3 mM apo protein in UB 7 and 1.2 mM $CuSO_4$ premixed with glycerol to give a final concentration of 1.5 mM protein, 0.6 mM $CuSO_4$. For longer time point samples (5 min – 24 hours), a pool of apo protein and $CuSO_4$ was mixed together, stirred at 10°C while aliquots from the mixture were frozen at desired time points to monitor either the decay of I_x, or formation of T1Cu intermediate or the formation of the final Cu_A form, after adding glycerol to a final concentration of 22%. All samples for longer time points had the same starting concentrations of apo protein and $CuSO_4$ as the samples frozen at the earliest time points, to be consistent. Pure holo Cu_A forms of each variant were prepared by adding a solution of premixed 0.8 eq. Cu(I) and 0.8 eq. $CuSO_4$ to the apo protein in UB 7. Sub-stoichiometric Cu was added to ensure no excess Cu is present in solution. Cu(I) was added in the form of tetrakis(acetonitrile)copper(I)hexafluorophosphate. Experimental EPR data were simulated using SIMPOW6.[64] All the spectra were fit simultaneously to obtain relative populations and EPR parameters of various species so as to minimize the total rms difference between experimental and simulated spectra. For spin quantification, $CuSO_4$ standards were prepared at concentrations ranging from 2 – 0.0625 mM. EPR data for the standards and the protein samples were collected at a constant temperature and power of 30K, and 0.2 mW, respectively. Instrument gain was normalized across all samples. Standard curve was obtained by plotting the double integration area as a function of $CuSO_4$ concentration. Cu(II) concentration in protein samples were calculated from the standard curve.

X-ray Absorption Spectroscopy

The Extended X-ray Absorption Fine Structure (EXAFS) spectra were collected at beam line X3B, National Synchrotron Light Source with a sagittally focused Si (111) crystal monochromator. Samples were cooled to 10K before scanning and kept cold during data collection. Kα fluorescence was collected by a Canberra 31-element Ge detector. A Cu foil was used as reference to calibrate energy. A 6μm Ni filter was placed before detector to reduce elastic scattering. Six scans of each sample were collected. These samples were prepared using similar procedure as described in the EPR section. Samples contained 5.2 – 5.8 mM apo protein in UB 7, 2.08–2.32 mM $CuSO_4$ [1:0.4 ratio of apo protein to Cu(II)] to a final concentration and flash frozen in liquid N_2 at various time points (50 s – 10 hours) after adding 20% ethylene glycol as the glassing agent. For earliest time points (50s – 60s) ethylene glycol and $CuSO_4$ were premixed prior to adding to the apo protein. Data reduction and background subtraction were performed with EXAFSPAK[65] and data was fitted with EXCURVE 9.2.[66]

Results and Discussions

Kinetics of Cu_A Reconstitution in Glu114Gly/Ala/Leu/GlnCu_AAz

The kinetic processes of Cu_A reconstitution in Glu114Gly/Ala/Leu/GlnCu_AAz were monitored by stopped flow and standard UV-vis absorption spectroscopy in the presence of sub-equivalent amounts of $CuSO_4$. Addition of 0.4 eq. $CuSO_4$ to 0.25 mM Glu114GlyCu_AAz led to the formation, within 100 ms, of a species displaying an intense peak at 390 nm and a weak absorption peak at ~625 nm (Fig. 2A). The intense absorption

centered at 390 nm is characteristic of the $S_{Cys(\sigma)}\rightarrow Cu(II)$ charge transfer (CT) transition of a red T2Cu species.[10, 59] Over the next 50s, an intermediate species formed exhibiting two intense $S_{Cys}\rightarrow Cu$ CT transitions at 413 nm (sharp) and 616 nm (broad), plus a broad peak at 762 nm. These features are similar to the previously reported intermediate X (I_x).[59] The 413 nm peak formed faster than the 616 nm peak over the next 14 minutes, and also decayed faster. At the end of 14 minutes, the 413 nm peak red shifted to 420 nm, and the 616 nm peak blue shifted to ~610 nm, indicating the formation of blue T1Cu species. Over the next 5 hours, as monitored using separate kinetic UV-vis experiments (see materials and methods for details) the intense absorption bands at 420 and 610 nm attributable to T1Cu decayed, and the peaks for Cu_A at 478 nm, 534 nm, and 795 nm (Fig. 2A, inset) fully developed. Unlike other variants (*vide infra*), the kinetic processes of Glu114GlyCu_AAz did not display any isosbestic point at any time point. Analysis of the stopped flow data (1000 s) was performed using a kinetic model involving the formation of the early red T2Cu intermediate followed by the formation of I_x and the T1Cu (Fig. S1, Table 1).

Next we investigated the kinetics of Cu incorporation into the Glu114AlaCu_AAz variant. Similar to Glu114GlyCu_AAz, an early red T2Cu intermediate formed within 134 ms with an absorption band occurring at ~362 nm (Fig. 2B). A new intermediate species, corresponding to I_x, formed within the next 50 s, with intense peaks at 412 nm and 624 nm, and a broad feature at ~774 nm. This process was accompanied by an isosbestic point occurring at 390 nm. The intensity of the 412 nm peak was higher than that of the 624 nm peak. A small amount of Cu_A was also present. In the next ~900 s, the 412 nm peak decreased in intensity and red shifted to 426 nm, while the 624 nm peak blue shifted to 616 nm, with a concomitant increase in intensity. The new features are attributed to a blue T1Cu species that developed with isosbestic conversion from I_x. The 426 and 616 nm peaks of the T1Cu intermediate decayed over the next 10 hours, while absorptions in the regions typical of Cu_A increased, with isosbestic points occurring at 460 nm, and 556 nm (Fig. 2B, inset). The kinetic processes within the first 1000 s were modeled (Fig. S1, Table 1) similar to that of Glu114GlyCu_AAz.

For Glu114LeuCu_AAz, a red T2Cu intermediate with an intense absorption peak appearing at ~360 nm was also formed within 100 ms of mixing, (Fig. 2C), which decayed to I_x within 60 s with isosbestic point at 387 nm. The I_x displayed two intense absorption peaks at 413 nm, 470 nm, and a broad feature at ~793 nm. The intensity of the 413 nm peak was higher than that of the 470 nm peak. The I_x started to decay after 85 s, and was converted to a blue T1Cu intermediate with peaks occurring at 467 nm, 614 nm and a weak band at 793 nm and isosbestic points at 560 nm, and 680 nm. The T1Cu was fully formed within 40 min and started to decay to Cu_A with an isosbestic point at 560 nm over 10 hours (Fig. 2C, inset). The stopped flow data were modeled in the same way as other variants (Fig. S1, Table 1).

Finally, in Glu114GlnCu_AAz, a red T2Cu intermediate displaying an intense peak at ~385 nm was observed within 100 ms of mixing (Fig. 2D). Within 50 s the I_x formed displaying two intense absorption bands at 409 nm, 470 nm, and a broad peak at ~790 nm with an isosbestic point at 390 nm. The 409 nm peak is slightly higher in intensity than the 470 nm peak. The I_x decayed to a blue T1Cu intermediate with isosbestic points at 572 nm and 653 nm. The T1Cu intermediate having peaks at 467 nm, 601 nm, and ~790 nm fully developed

within 20 min. After 30 min from mixing, Cu_A started to form having a weak peak at ~351 nm, two intense peaks at 479 nm, 541 nm, and a broad feature at ~760 nm, formed with isosbestic points at 434 nm, and 531 nm. The full Cu_A formation was observed within 10 hours (Fig. 2D, inset). The kinetic processes in the first 1000 s were modeled as others (Fig. S1, Table 1).

Since no external reductant was added and the formation of the mixed valence Cu_A site requires Cu(I), the reducing equivalents must be supplied by the active site cysteines. To investigate the effect of oxygen on the overall kinetic processes, we performed stopped-flow experiments under O_2-free and O_2-rich conditions. The results showed that, in the absence of O_2, no T1Cu intermediate was formed in any of the mutants, whereas under O_2-rich condition, the rate of T1Cu formation from I_x was faster compared to normal atmospheric O_2 levels (Fig. S2, Table S1). These observations suggest a role of O_2 in the formation of the T1Cu species. The absorption at ~625 nm for I_x of Glu114Gly/Ala/Cu_AAz bears a strong resemblance to the T1Cu species that forms at latter time points. However, this peak is also present under anaerobic conditions, where the T1Cu species does not form, suggesting that this peak does indeed belong to the I_x of the G and A variants.

Effect of Glu114 Substitutions on the Rates of Formation and the Characteristics of the Intermediates

It has been previously proposed that the formation of the initial capture complex for Cu ion involves Cys116 as the Cu ligand close to the exterior of the protein.[59] Our results indicate that the initial rates of formation of the red T2Cu capture complex are quite similar in all the four variants (Table 1, Fig. 3A), suggesting that substitution of the Glu114 side chain has minimal effect on the formation of the capture complex. However, the rate of the formation of I_x from the red T2Cu complex is fastest in Glu114GlyCu_AAz (Fig. 3B, Table 1) among the four variants. In the previous study,[59] the formation of I_x from the T2Cu capture complex was proposed to involve a conformational change of the Cu_A loop, where the Cu-bound Cys116 reoriented from the protein exterior to the interior. Our results herein support this hypothesis, as the conformational change of the Cu_A loop required for the formation of I_x would be most favorable in Glu114GlyCu_AAz, because Gly has the least steric side chain and most flexible backbone conformation in the Ramachandran plot.[67] The presence of longer side chain groups in Ala, Leu, Gln or Glu would accordingly disfavor such a conformational change, owing to steric encumbrance from these side chains and less backbone flexibility. Taken together, these results suggest that the backbone flexibility is an important factor in determining the rates of T2Cu→I_x formation. In a related study involving *Tt* Cu_A the presence of a hydrophobic patch involving Leu155 in the metal binding loop was shown to be important in facilitating ET between cytochrome c_{552} and the *Tt* Cu_A.[68]

The kinetic data further suggest that the nature of the Glu114 side chain influences the timescales on which these intermediates are formed, the wavelengths of the absorption peaks, and how cleanly one intermediate is converted to another. For example, in Glu114GlyCu_AAz, no isosbestic point was observed during any of the kinetic processes, whereas, in the other three variants, well-defined isosbestic points were observed for conversions between different species. The cleanest conversion from one intermediate to

another was observed in Glu114LeuCu$_A$Az, and Glu114GlnCu$_A$Az, where minimal spectral overlap among different species was present. In contrast, a strong overlap between the I_x, and T1Cu intermediates was observed in the other two variants. Interestingly, the split peaks for the I_x at 410, and 470 nm were observed only in Glu114LeuCu$_A$Az, and Glu114GlnCu$_A$Az. Additionally, the relative intensities of these two peaks are reversed in Glu114LeuCu$_A$Az, and Glu114GlnCu$_A$Az, where the 410 nm peak is more intense in the former, whereas the 470 nm peak has higher intensity in the latter variant. These observations, therefore, indicate that Glu114 side chain plays a role in dictating the characteristics of the intermediates.

EPR Studies of the I_x species

To further understand the nature of the intermediates, in particular, I_x, we collected X-band EPR data of two representative variants, the Glu114GlyCu$_A$Az that did not display kinetic isosbestic point and Glu114GlnCu$_A$Az that did. The EPR spectrum of Glu114GlyCu$_A$Az collected at 50s (the time point at which the I_x formed with maximum population) (Fig. 4a) was simulated as two mononuclear Cu(II) species in almost equal population (38% and 46%, respectively). From the simulations, the g_z and A_z values for the two I_x were extracted to be 2.152, 101×10^{-4} cm^{-1}, for I_{x1}, and 2.185, 90×10^{-4} cm^{-1} (Table 2) for I_{x2}, respectively. While the Z-components of hyperfine couplings (A_z) are similar in both I_{x1} and I_{x2} that fall in between those of T1Cu and T2Cu complexes, their g_z values differ significantly from each other.[10, 69] A smaller g_z value in I_{x1} suggests that the strength of the thiolate-Cu interaction is slightly stronger in I_{x1} in comparison to I_{x2}. Both the g_z and A_z for I_{x1} is similar to the Sco protein (g_z=2.150).[45] In addition, the A_z value is similar to the intermediate observed in *Tt* Cu$_A$ (A_z = 109 × 10^{-4} cm^{-1}).[56] In both of these systems, copper is present as a bis-thiolate Cu(Cys)$_2$His complex. By analogy, we assign the I_{x1} having a similar ligand environment to these two Cu(II) centers. The I_{x2} with a g_z of 2.185 is lower than most T1Cu sites (g_z ~2.190–2.300).[10] The I_{x2} can be best assigned as having a slightly different ligand coordination/geometry around the metal site relative to that of I_{x1}.

For Glu114GlnCu$_A$Az, two mononuclear Cu(II) species were also observed at 50 s (time point at which the I_x formed with maximum population), but with unequal populations of 68% and 18%, respectively (Fig. 4b). The first species has a g_z of 2.151 and A_z of 82×110^{-4} cm^{-1} (Table 2), which is indicative of a species with a strong thiolate-Cu interaction and can be assigned as I_{x1} with Cu(Cys)$_2$His ligation, using a similar analogy to the I_{x1} of Glu114GlyCu$_A$Az. The second species, I_{x2}, present in 18% population, has a g_z of 2.249 and A_z of 133×10^{-4} cm^{-1}. Although both the g_z and A_z values are higher than the I_{x2} of Glu114GlyCu$_A$Az, these parameters are similar to the Cu(Cys)$_2$(His)L (L=pyrazole, NADH) complex of HLADH (g_z=2.200, A_z=115 × 10^{-4} cm^{-1}).[60–62] Based on this similarity, we assign the I_{x2} of Glu114GlnCu$_A$Az as having a similar Cu(Cys)$_2$(His)L (L=weak axial ligand) ligation/geometry.

These EPR data also suggest that a small amount of Cu$_A$ is formed along with the I_x (Table S2). Subsequently, the I_x decayed and more T1Cu and Cu$_A$ formed (see the SI). The pure Cu$_A$ forms of each variant show the expected well-resolved seven-line hyperfine pattern, as well as the characteristic EPR parameters (Fig. S3 Table S3).

X-ray Absorption Spectroscopy

To probe the ligand and coordination environment of the I_x, Cu k edge X-ray absorption spectroscopy was used. The EXAFS data for the I_x of Glu114GlyCu_AAz was best simulated as 2 Cu-S_{Cys} ligands at 2.17 Å, and 1 Cu-N_{His} ligand at 1.97 Å (Fig. 5A, Table 3). For Glu114GlnCu_AAz, the EXAFS data (Fig. 5B) for the I_x was best simulated as 1 Cu-N_{His} at 1.93 Å, and 2 Cu-S_{Cys} at 2.20 Å (Table 3). According to EPR simulation, two I_x species are present at this time point with slightly different ligand geometry (*vide supra*). However, as EXAFS measures average Cu-ligand distances, the individual Cu(II) species cannot be deconvoluted from the EXAFS data.

In the I_x of these variants the $Cu(Cys)_2His$ ligand coordination is similar to what was observed for the green intermediate in *Tt* Cu_A as well as for the Sco protein.[45, 56, 59] The EXAFS spectra and data analysis of the holo Cu_A samples of the Glu114XCu_AAz variants are consistent with other reported Cu_A systems (Fig. S4, Table S4).[56]

Proposed Mechanism of Cu_A Formation

The combined UV-vis, EPR, and EXAFS data presented in this work has allowed us to propose a mechanism of Cu_A formation in these Cu_AAz variants (Scheme 1). Upon addition of sub-equivalent Cu(II) to the apo proteins, an initial red T2Cu capture complex is formed within ~100 ms. Previous results from Cu_AAz established that the T2Cu capture complex is formed close to the exterior of the protein with Cys116 as the only protein-derived ligand.[44, 59] The next step of the mechanism is bifurcated (Scheme 1): conversion of T2Cu to I_x, and formation of a small population of Cu_A in a direct pathway from the T2Cu complex. Previously, it was hypothesized that T2Cu to I_x formation involved a conformation change of the Cu_A loop by which the capture complex is internalized from the protein exterior. Our results in this work show that T2Cu to I_x formation is fastest in Glu114GlyCu_AAz compared to the other mutants. As Gly has the most flexible backbone conformation, this observation, therefore, supports the hypothesis that indeed T2Cu to I_x formation is facilitated by swinging of the Cu_A loop, which brings the Cu to the protein interior.

In the next step the I_x decay and T1Cu complexes form within ~15 minutes. The formation of T1Cu complex is dependent on the presence of O_2, as the T1Cu species does not form in the absence of O_2 (Fig. S2). Since, in all cases, the decay of I_x is accompanied by the formation of the T1Cu species in the presence of O_2, it can be inferred that the T1Cu complex is a result of the oxidation of the decay product of I_x. EPR spin quantification shows that the I_x of Glu114GlyCu_AAz decay with time (Fig. S5), indicating spin loss due to the formation of the EPR silent Cu(I) species. Therefore, the T1 Cu is a product of the oxidation of Cu(I) formed during the decay of I_x. At even longer time scale, the T1Cu complex decays and Cu_A start to form (Fig. 2, insets). Formation of the binuclear Cu_A from T1Cu complexes must be achieved by reaction of the T1Cu species with either free Cu(I) generated *in situ* or with Cu(I)-Cu_AAz.

The formation of a small population of Cu_A from T2Cu as observed here must be achieved by reaction of free Cu(I) with the Cu(II)-loaded protein. As no external reductant was added,

the Cu(I) must be generated *in situ* by the reduction of Cu(II) to Cu(I) by the active site cysteines of an apo Cu_A site. As the oxidation of cysteines to cystine is a $2e^-$ process, more than one Cu(II)-bound proteins must be interacting with each other to receive the reducing equivalents from the cysteine thiols. Alternatively, Cu(I) may also be generated by the reaction of free Cu(II) with the I_x, as suggested in the case of *Tt* Cu_A system.[56] It is highly unlikely that nature only uses Cu(II) to metallate the Cu_A sites as it would be a significant waste of apo proteins to supply the reducing equivalents. Using both Cu(II) and Cu(I) would make the metallation process much more efficient as also shown in *Tt* Cu_A.[56] The yield of holo Cu_A in the Glu114XCu_AAz variants significantly increased while using a mixture of Cu(II) and Cu(I) (Table S3).

Identity of Intermediate X (I_x)

A major focus of this study is to determine the ligand and coordination environment of the I_x using the Glu114XCu_AAz variants. In the previous kinetic study of Cu_AAz, at the time when the I_x was formed with maximum population (~55% at ~30s), significant populations of other types of Cu species (Cu_A', T1Cu) were present.[59] As a result, the identity of this species could not be experimentally determined. In contrast, the I_x in these Cu_A variants presented here can be obtained with a maximum of ~80–85% combined population, with only a minor percentage of Cu_A coexisting with the I_x. The electronic absorption data of the Glu114XCu_AAz variants indicate two sharp peaks in the 410–600 nm region and a broad feature at ~700–800 nm, similar to the pyrazole-substituted HLADH, which displays two peaks at ~400–500 nm, and a broad feature ~600–800 nm.[60–62] The EPR results indicate the presence of mononuclear T2Cu species with thiolate ligands. In all the variants, the EPR data suggest two mononuclear Cu complexes with minor differences in ligand coordination/geometry. Comparing the EPR parameters of the I_{x1} to the green intermediate in *Tt* Cu_A and Cu(II)-Sco proteins (Table 2), the I_{x1} intermediate observed in the Glu114GlyCu_AAz, and Glu114GlnCu_AAz variants can be best described as $Cu(Cys)_2(His)$ complexes in trigonal geometry, while the I_{x2} can be best described as $Cu(Cys)_2(His)L$ (L = weak axial ligand) complex in distorted tetrahedral geometry. The proposed ligands and geometries are consistent with EXAFS data, which can be modeled as 3-coordinate mononuclear $Cu(Cys)_2His$ complex. Therefore, a combined UV-Vis, EPR, and EXAFS data indicate the presence of Cu-bisthiolato complexes with slightly different ligation/geometry as the identity of these intermediates (Fig. 6).

Conclusions

We have investigated the influence of a key Cu_A ligand (Glu114) in Cu_A assembly as well as probed the nature of intermediates formed during *in vitro* reconstitution of the Cu_A center from Cu(II) ion and apo-forms of biosynthetic models in azurin (Cu_AAz). Our results show that the mechanism of Cu_A formation in variants of Glu114XCu_AAz (X=Gly, Ala, Leu, Gln) proceeds via an initial formation of a red T2Cu center followed by another mononuclear intermediate X (I_x), then a T1Cu intermediate and finally the binuclear Cu_A center. The results showed that the Glu114 backbone flexibility is an important factor in determining the rates of T2Cu→I_x formation, and suggest that Cu_A formation is facilitated by swinging of the ligand loop, which brings the external T2Cu complex to the protein interior. The kinetic

data further suggest that the nature of the Glu114 side chain influences the timescales on which these intermediates are formed, the wavelengths of the absorption peaks, and how cleanly one intermediate is converted to another. This mechanistic investigation allowed us to find optimal conditions to obtain a high population of the I_x intermediate (80–85%), facilitating the use of UV-vis, EPR and EXAFS to elucidate the structure of I_x, which is best described as $Cu(Cys)_2(His)$ complex in trigonal geometry. While similar intermediates and mechanisms have been identified in native Cu_A, the exact structural features and pathways for the Cu_A formation are still not well understood. Our findings here of the mechanistic steps and the identification of key mononuclear intermediates during the assembly of the biosynthetic models of Cu_A in azurin and its variants have shed light into the mechanism of Cu_A formation.

Supplementary Material

Refer to Web version on PubMed Central for supplementary material.

Acknowledgments

Funding

This work was supported by the U.S. National Science Foundation (CHE-1413328 to Y.L. and NSF Graduate Research Fellowship DGE-0925180 to K.N.C.) and U. S. National Institutes of Health (GM054803 to N.J.B. and 5T32-GM070421 to J.R.), and the Howard Hughes Medical Institute Exceptional Research Opportunities Program (to M.J.P.). The EXAFS data were collected at beamline X3B of the National Synchrotron Light Source (NSLS) at Brookhaven National Laboratory. Beamline X3B at NSLS is operated by the Case Center for Synchrotron Biosciences, supported by NIH NIBIB grant P30-EB-009998. NSLS is supported by the U.S. Department of Energy, Office of Science, Office of Basic Energy Sciences, under Contract No. DE-AC02-98CH10886. The contents of this publication are solely the responsibility of the authors and do not necessarily represent the official views of NIGMS or NIH

We wish to thank Dr. Arnab Mukherjee for helpful discussions.

References

1. Liu J, Chakraborty S, Hosseinzadeh P, Yu Y, Tian S, Petrik I, Bhagi A, Lu Y. Metalloproteins Containing Cytochrome, Iron–Sulfur, or Copper Redox Centers. Chem Rev. 2014; 114:4366–4469. [PubMed: 24758379]
2. Gray HB, Malmström BG, Williams RJP. Copper coordination in blue proteins. J Biol Inorg Chem. 2000; 5:551. [PubMed: 11085645]
3. Vila, AJ.; Fernandez, CO. Copper in Electron Transfer Proteins. In: Bertini, I.; Sigel, A.; Sigel, H., editors. Handbook on Metalloproteins. Marcel Dekker; New York, NY: 2001. p. 813
4. Wilson TD, Yu Y, Lu Y. Understanding Copper-thiolate Containing Electron Transfer Centers by Incorporation of Unnatural Amino Acids and the CuA Center into the Type 1 Copper Protein Azurin. Coord Chem Rev. 2012; 257:260–276.
5. Lu, Y.; Chakraborty, S.; Miner, KD.; Wilson, TD.; Mukherjee, A.; Yu, Y.; Liu, J.; Marshall, NM. Metalloprotein Design. In: Reedijk, J.; Poeppelmeier, K., editors. Comprehensive Inorganic Chemistry II. Elsevier; Amsterdam: 2013. p. 565-593.
6. Chakraborty, S.; Hosseinzadeh, P.; Lu, Y. Metalloprotein Design and Engineering. In: Scott, RA., editor. Encyclopedia of Inorganic and Bioinorganic Chemistry. John Wiley and Sons, Ltd; Chichester: 2014. p. 1-51.
7. Farver, O.; Pecht, I. Prog Inorg Chem. John Wiley & Sons, Inc; 2008. Elucidation of Electron-Transfer Pathways in Copper and Iron Proteins by Pulse Radiolysis Experiments; p. 1-78.

8. Savelieff MG, Lu Y. Cu(A) centers and their biosynthetic models in azurin. J Biol Inorg Chem. 2010; 15:461–483. [PubMed: 20169379]
9. Solomon EI, Heppner DE, Johnston EM, Ginsbach JW, Cirera J, Qayyum M, Kieber-Emmons MT, Kjaergaard CH, Hadt RG, Tian L. Copper active sites in biology. Chem Rev. 2014; 114:3659–3853. [PubMed: 24588098]
10. Lu, Y. Electron transfer: Cupredoxins. In: Que, JL.; Tolman, WB., editors. Biocoordination Chemistry. Elsevier; Oxford, UK: 2004. p. 91-122.
11. Solomon EI. Spectroscopic Methods in Bioinorganic Chemistry: Blue to Green to Red Copper Sites. Inorg Chem. 2006; 45:8012–8025. [PubMed: 16999398]
12. Solomon EI, Xie X, Dey A. Mixed valent sites in biological electron transfer. Chem Soc Rev. 2008; 37:623–638. [PubMed: 18362972]
13. Tsukihara T, Aoyama H, Yamashita E, Tomizaki T, Yamaguchi H, Shinzawa-Itoh K, Nakashima R, Yaono R, Yoshikawa S. Structures of metal sites of oxidized bovine heart cytochrome c oxidase at 2.8 A. Science (Washington, DC, United States). 1995; 269:1069–1074.
14. Iwata S, Ostermeier C, Ludwig B, Michel H. Structure at 2.8 A resolution of cytochrome c oxidase from Paracoccus denitrificans. Nature. 1995; 376:660–669. [PubMed: 7651515]
15. Wikstrom M. Cytochrome c oxidase: 25 years of the elusive proton pump. Biochim Biophys Acta. 2004; 1655:241–247. [PubMed: 15100038]
16. Komorowski L, Anemuller S, Schafer G. First expression and characterization of a recombinant CuA-containing subunit II from an archaeal terminal oxidase complex. J Bioenerg Biomembr. 2001; 33:27–34. [PubMed: 11460923]
17. Komorowski L, Schafer G. Sulfocyanin and subunit II, two copper proteins with novel features, provide new insight into the archaeal SoxM oxidase supercomplex. FEBS Lett. 2001; 487:351–355. [PubMed: 11163357]
18. Brown K, Tegoni M, Prudencio M, Pereira AS, Besson S, Moura JJ, Moura I, Cambillau C. A novel type of catalytic copper cluster in nitrous oxide reductase. Nat Struct Biol. 2000; 7:191–195. [PubMed: 10700275]
19. Zumft WG, Kroneck PMH. Respiratory transformation of nitrous oxide (N2O) to dinitrogen by Bacteria and Archaea. Adv Microb Physiol. 2007; 52:107–227. [PubMed: 17027372]
20. Suharti Strampraad MJ, Schröder I, de Vries S. A Novel Copper A Containing Menaquinol NO Reductase from Bacillus azotoforman s. Biochemistry. 2001; 40:2632–2639. [PubMed: 11327887]
21. Gamelin DR, Randall DW, Hay MT, Houser RP, Mulder TC, Canters GW, de VS, Tolman WB, Lu Y, Solomon EI. Spectroscopy of Mixed-Valence CuA-Type Centers: Ligand-Field Control of Ground-State Properties Related to Electron Transfer. J Am Chem Soc. 1998; 120:5246–5263.
22. Neese F, Zumft WG, Antholine WE, Kroneck PMH. The Purple Mixed-Valence CuA Center in Nitrous-oxide Reductase: EPR of the Copper-63-, Copper-65-, and Both Copper-65- and [15N]Histidine-Enriched Enzyme and a Molecular Orbital Interpretation. J Am Chem Soc. 1996; 118:8692–8699.
23. Olsson MH, Ryde U. Geometry, reduction potential, and reorganization energy of the binuclear Cu(A) site, studied by density functional theory. J Am Chem Soc. 2001; 123:7866–7876. [PubMed: 11493060]
24. Hulse CL, Averill BA. Isolation of a high specific activity pink, monomeric nitrous oxide reductase from Achromobacter cycloclastes. Biochem Biophys Res Commun. 1990; 166:729–735. [PubMed: 2154217]
25. Lappalainen P, Aasa R, Malmstrom BG, Saraste M. Soluble CuA-binding domain from the Paracoccus cytochrome c oxidase. J Biol Chem. 1993; 268:26416–26421. [PubMed: 8253767]
26. Slutter CE, Sanders D, Wittung P, Malmstrom BG, Aasa R, Richards JH, Gray HB, Fee JA. Water-soluble, recombinant CuA-domain of the cytochrome ba3 subunit II from Thermus thermophilus. Biochemistry. 1996; 35:3387–3395. [PubMed: 8639488]
27. von Wachenfeldt C, de Vries S, van der Oost J. The CuA site of the caa3-type oxidase of Bacillus subtilis is a mixed-valence binuclear copper center. FEBS Lett. 1994; 340:109–113. [PubMed: 8119391]
28. Arciero DM, Hooper AB, Rosenzweig AC. Crystal Structure of a Novel Red Copper Protein from Nitrosomonas europaea. Biochemistry. 2001; 40:5674–5681. [PubMed: 11341832]

29. Arciero DM, Pierce BS, Hendrich MP, Hooper AB. Nitrosocyanin, a red cupredoxin-like protein from Nitrosomonas europaea. Biochemistry. 2002; 41:1703–1709. [PubMed: 11827513]
30. Ryden LG, Hunt LT. Evolution of protein complexity: the blue copper-containing oxidases and related proteins. J Mol Evol. 1993; 36:41–66. [PubMed: 8433378]
31. Savelieff MG, Wilson TD, Elias Y, Nilges MJ, Garner DK, Lu Y. Experimental evidence for a link among cupredoxins: red, blue, and purple copper transformations in nitrous oxide reductase. Proc Natl Acad Sci. 2008; 105:7919–7924. [PubMed: 18535143]
32. Farrar JA, Lappalainen P, Zumft WG, Saraste M, Thomson AJ. Spectroscopic and mutagenesis studies on the CuA centre from the cytochrome-c oxidase complex of Paracoccus denitrificans. Eur J Biochem. 1995; 232:294–303. [PubMed: 7556164]
33. Maneg O, Ludwig B, Malatesta F. Different Interaction Modes of Two Cytochrome-c Oxidase Soluble CuA Fragments with Their Substrates. J Biol Chem. 2003; 278:46734–46740. [PubMed: 12937163]
34. Paumann M, Lubura B, Regelsberger G, Feichtinger M, Koellensberger G, Jakopitsch C, Furtmueller PG, Peschek GA, Obinger C. Soluble CuA Domain of Cyanobacterial Cytochrome c Oxidase. J Biol Chem. 2004; 279:10293–10303. [PubMed: 14672950]
35. Slutter CE, Langen R, Sanders D, Lawrence SM, Wittung P, Di Bilio AJ, Hill MG, Fee JA, Richards JH, et al. Electron-transfer studies with the CuA domain of Thermus thermophilus cytochrome ba3. Inorg Chim Acta. 1996; 243:141–145.
36. Williams PA, Blackburn NJ, Sanders D, Bellamy H, Stura EA, Fee JA, McRee DE. The CuA domain of Thermus thermophilus ba3-type cytochrome c oxidase at 1.6 Å resolution. Nat Struct Biol. 1999; 6:509–516. [PubMed: 10360350]
37. Dennison C, Vijgenboom E, de Vries S, van der Oost J, Canters GW. Introduction of a CuA site into the blue copper protein amicyanin from Thiobacillus versutus. FEBS Lett. 1995; 365:92–94. [PubMed: 7774723]
38. Hay M, Richards JH, Lu Y. Construction and characterization of an azurin analog for the purple copper site in cytochrome c oxidase. Proc Natl Acad Sci. 1996; 93:461. [PubMed: 8552661]
39. Jones LH, Liu A, Davidson VL. An Engineered CuA Amicyanin Capable of Intermolecular Electron Transfer Reactions. J Biol Chem. 2003; 278:47269–47274. [PubMed: 12970350]
40. van der Oost J, Lappalainen P, Musacchio A, Warne A, Lemieux L, Rumbley J, Gennis RB, Aasa R, Pascher T, Malmstrom BG. Restoration of a lost metal-binding site: construction of two different copper sites into a subunit of the E. coli cytochrome o quinol oxidase complex. EMBO J. 1992; 11:3209–3217. [PubMed: 1324168]
41. Farver O, Lu Y, Ang MC, Pecht I. Enhanced rate of intramolecular electron transfer in an engineered purple CuA azurin. Proc Natl Acad Sci. 1999; 96:899–902. [PubMed: 9927665]
42. Hay MT, Ang MC, Gamelin DR, Solomon EI, Antholine WE, Ralle M, Blackburn NJ, Massey PD, Wang X, Kwon AH, Lu Y. Spectroscopic Characterization of an Engineered Purple CuA Center in Azurin. Inorg Chem. 1998; 37:191–198.
43. Hwang HJ, Berry SM, Nilges MJ, Lu Y. Axial Methionine Has Much Less Influence on Reduction Potentials in a CuA Center than in a Blue Copper Center. J Am Chem Soc. 2005; 127:7274–7275. [PubMed: 15898751]
44. Hwang HJ, Nagraj N, Lu Y. Spectroscopic Characterizations of Bridging Cysteine Ligand Variants of an Engineered Cu2(SCys)2 CuA Azurin. Inorg Chem. 2006; 45:102–107. [PubMed: 16390045]
45. Andruzzi L, Nakano M, Nilges MJ, Blackburn NJ. Spectroscopic studies of metal binding and metal selectivity in Bacillus subtilis BSco, a homologue of the yeast mitochondrial protein Sco1p. J Am Chem Soc. 2005; 127:16548–16558. [PubMed: 16305244]
46. Banci L, Bertini I, Cavallaro G, Ciofi-Baffoni S. Seeking the determinants of the elusive functions of Sco proteins. FEBS J. 2011; 278:2244–2262. [PubMed: 21518258]
47. Horng YC, Cobine PA, Maxfield AB, Carr HS, Winge DR. Specific copper transfer from the Cox17 metallochaperone to both Sco1 and Cox11 in the assembly of yeast cytochrome C oxidase. J Biol Chem. 2004; 279:35334–35340. [PubMed: 15199057]
48. Nittis T, George GN, Winge DR. Yeast Sco1, a Protein Essential for Cytochrome cOxidase Function Is a Cu (I)-binding Protein. J Biol Chem. 2001; 276:42520–42526. [PubMed: 11546815]

49. Balatri E, Banci L, Bertini I, Cantini F, Ciofi-Baffoni S. Solution structure of Sco1: a thioredoxin-like protein involved in cytochrome c oxidase assembly. Structure. 2003; 11:1431–1443. [PubMed: 14604533]
50. Banci L, Bertini I, Calderone V, Ciofi-Baffoni S, Mangani S, Martinelli M, Palumaa P, Wang S. A hint for the function of human Sco1 from different structures. Proc Natl Acad Sci. 2006; 103:8595–8600. [PubMed: 16735468]
51. Horng YC, Leary SC, Cobine PA, Young FB, George GN, Shoubridge EA, Winge DR. Human Sco1 and Sco2 function as copper-binding proteins. J Biol Chem. 2005; 280:34113–34122. [PubMed: 16091356]
52. Siluvai GS, Nakano M, Mayfield M, Blackburn NJ. The essential role of the Cu (II) state of Sco in the maturation of the CuA center of cytochrome oxidase: evidence from H135Met and H135SeM variants of the Bacillus subtilis Sco. J Biol Inorg Chem. 2011; 16:285–297. [PubMed: 21069401]
53. Siluvai GS, Nakano MM, Mayfield M, Nilges MJ, Blackburn NJ. H135A controls the redox activity of the Sco copper center. Kinetic and spectroscopic studies of the His135Ala variant of Bacillus subtilis Sco. Biochemistry. 2009; 48:12133–12144. [PubMed: 19921776]
54. Abriata LA, Banci L, Bertini I, Ciofi-Baffoni S, Gkazonis P, Spyroulias GA, Vila AJ, Wang S. Mechanism of CuA assembly. Nat Chem Biol. 2008; 4:599–601. [PubMed: 18758441]
55. Siluvai GS, Mayfield M, Nilges MJ, DeBeer George S, Blackburn NJ. Anatomy of a red copper center: spectroscopic identification and reactivity of the copper centers of Bacillus subtilis Sco and its Cys-to-Ala variants. J Am Chem Soc. 2010; 132:5215–5226. [PubMed: 20232870]
56. Chacón KN, Blackburn NJ. Stable Cu (II) and Cu (I) mononuclear intermediates in the assembly of the CuA center of Thermus thermophilus cytochrome oxidase. J Am Chem Soc. 2012; 134:16401–16412. [PubMed: 22946616]
57. Ghosh MK, Basak P, Mazumdar S. Mechanism of Copper Incorporation in Subunit II of Cytochrome c Oxidase from Thermus thermophilus: Identification of Intermediate Species. Biochemistry. 2013; 52:4620–4635. [PubMed: 23745508]
58. Wang X, Ang MC, Lu Y. Kinetics of Copper Incorporation into an Engineered Purple Azurin. J Am Chem Soc. 1999; 121:2947–2948.
59. Wilson TD, Savelieff MG, Nilges MJ, Marshall NM, Lu Y. Kinetics of Copper Incorporation into a Biosynthetic Purple CuA Azurin: Characterization of Red, Blue, and a New Intermediate Species. J Am Chem Soc. 2011; 133:20778–20792. [PubMed: 21985501]
60. Farrar JA, Formicka G, Zeppezauer M, Thomson AJ. Magnetic and optical properties of copper-substituted alcohol dehydrogenase: a bisthiolate copper(II) complex. Biochem J. 1996; 317:447–456. [PubMed: 8713071]
61. Maret W, Dietrich H, Ruf HH, Zeppezauer M. Active Site-Specifc Reconstituted Copper (II) Horse Liver Alcohol Dehydrogenase: A Biological Model for Type 1 Cu2+ and its Changes Upon Ligand Binding and Confnrmational Transitions. J Inorg Biochem. 1980; 12:241–252. [PubMed: 6247444]
62. Maret W, Kozlowski H. Biochim Biophys Acta. 1987; 912:329. [PubMed: 3032263]
63. Robinson H, Ang MC, Gao Y-G, Hay MT, Lu Y, Wang AHJ. Structural Basis of Electron Transfer Modulation in the Purple CuA Center. Biochemistry. 1999; 38:5677–5683. [PubMed: 10231517]
64. Nilges, MJ.; Matteson, K.; Belford, RL. SIMPOW6: A software package for the simulation of ESR powder-type spectra. In: Hemminga, MA.; Berliner, L., editors. ESR Spectroscopy in Membrane Biophysics. Vol. 27. Springer; New York: 2006.
65. George, GN. EXAFSPAK. Stanford Synchrotron Radiation Laboratory; Menlo Park, CA: 1995.
66. Gurman S, Binsted N, Ross I. A rapid, exact, curved-wave theory for EXAFS calculations. II The multiple-scattering contributions. J Phys C: Solid State Phys. 1986; 19:1845.
67. Ramachandran GN, Ramakrishnan C, Sasisekharan V. Stereochemistry of polypeptide chain configurations. J Mol Biol. 1963; 7:95–99. [PubMed: 13990617]
68. Ghosh MK, Rajbongshi J, Basumatary D, Mazumdar S. Role of the Surface-Exposed Leucine 155 in the Metal Ion Binding Loop of the CuA Domain of Cytochrome c Oxidase from Thermus thermophilus on the Function and Stability of the Protein. Biochemistry. 2012; 51:2443–2452. [PubMed: 22372469]

69. Solomon EI, Szilagyi RK, DeBeer George S, Basumallick L. Electronic Structures of Metal Sites in Proteins and Models: Contributions to Function in Blue Copper Proteins. Chem Rev. 2004; 104:419–458. [PubMed: 14871131]

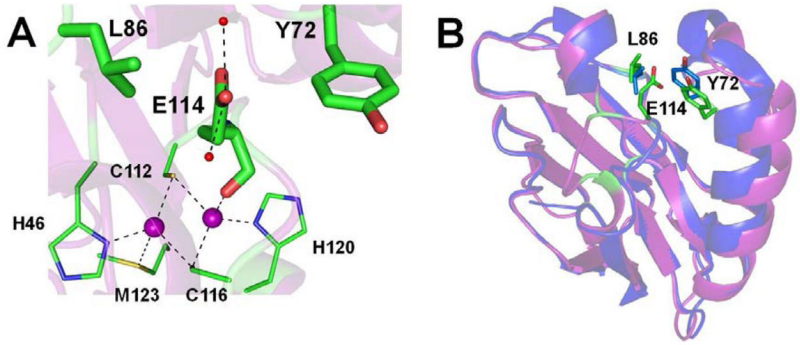

Figure 1.

A. Orientation of the Glu114 side chain in Cu_AAz in between the two hydrophobic amino acids L86 and Y72, shown as sticks. Cu_A ligands are shown as lines, Cu atoms as purple spheres, water molecules that form hydrogen bonding interactions with the Glu114 side chain are shown as red spheres. Protein backbone is shown as cartoon. **B.** Cartoon representation of Cu_AAz (purple), and blue Cu Az (blue) showing how the placement of Glu114 side chain in Cu_AAz sterically pushes the two helices that house L86, and Y72, compared to the blue Cu Az. Figures were generated in PyMol.

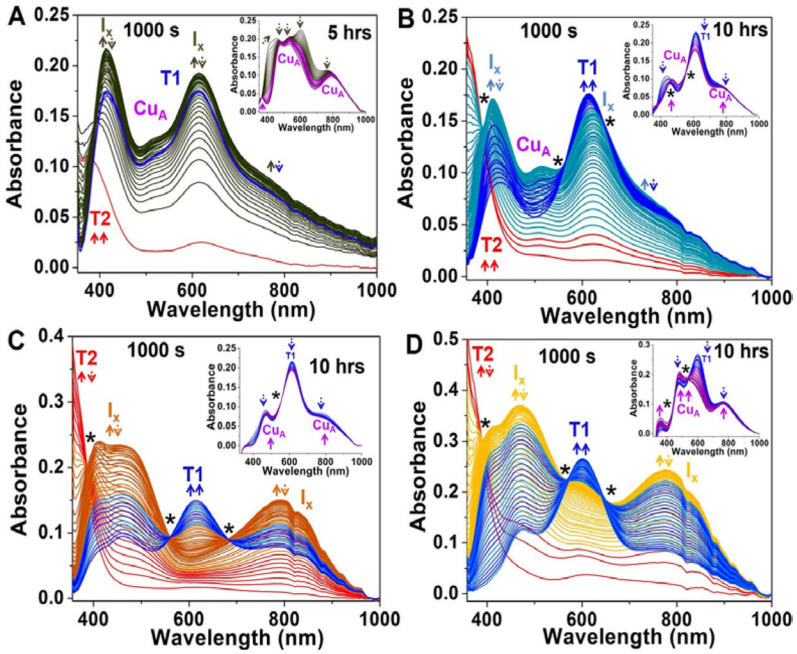

Figure 2.

Stopped-flow spectra obtained after mixing 0.5 mM apo Glu114GlyCu$_A$Az (**A**), Glu114AlaCu$_A$Az (**B**), Glu114LeuCu$_A$Az (**C**), and Glu114GlnCu$_A$Az (**D**) in UB 7 buffer, with 0.2 mM $CuSO_4$. Insets show separate kinetic UV-vis experiments under the same condition, monitored for longer time. Isosbestic points are shown as asterisks (*). Unique UV-vis signatures for individual I_x (I_{x1}, and I_{x2}) as seen by EPR (*vide infra*) cannot be deconvoluted due to spectral overlap and are labeled as I_x. Up and down arrows indicate the formation and decay of various species.

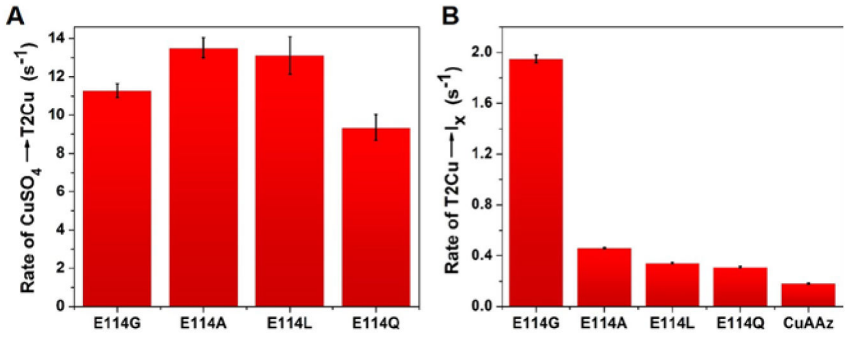

Figure 3.

A) Rates of $CuSO_4 \rightarrow T2Cu$, and **B)** $T2Cu \rightarrow I_x$ conversion of Cu_A variants obtained from the Stopped-flow data. Rates in **A)** are similar in all variants. In **B)** highest rate is observed for Glu114GlyCu_AAz which supports the hypothesis that the $T2Cu \rightarrow I_x$ conversion involves a conformation change of the Cu_A ligand loop as Gly has the most flexible backbone conformation, and thus favors such conformation change compared to the other amino acid side chains.

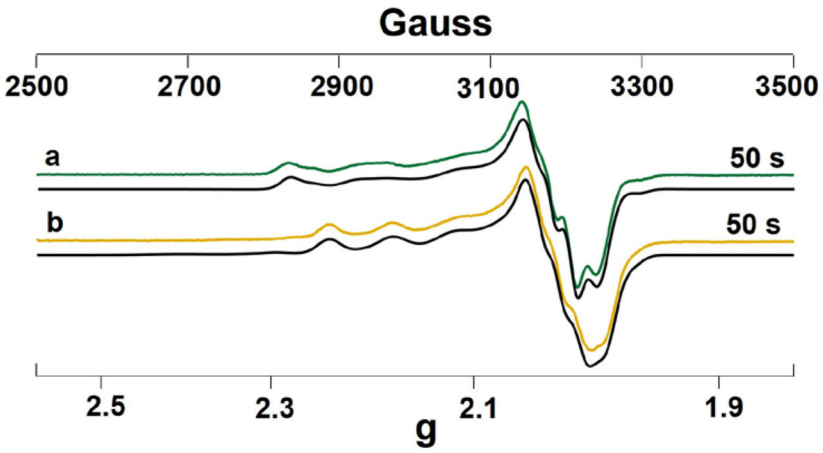

Figure 4.

X-band EPR spectra of samples containing 1.5 mM Glu114GlyCu_AAz (**a**), and Glu114GlnCu_AAz **(b)**, and 0.6 Mm $CuSO_4$, prepared at 50 s post-mixing. Experimental parameters: H = 9.053 GHz, T=30 K, Modulation = 4G, Microwave power = 0.2–0.5 mW. Simulated spectra are shown in black.

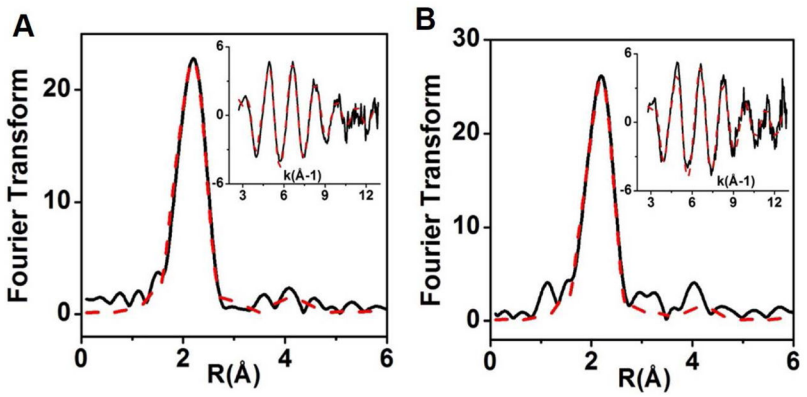

Fig. 5.

Fourier transform and EXAFS (inset) data of 50s samples of Glu114GlyCu_AAz (**A**), and Glu114GlnCu_AAz (**B**). Experimental data are shown as solid black lines and simulation are shown as dashed red lines. Parameters used to fit data are shown in Table 3.

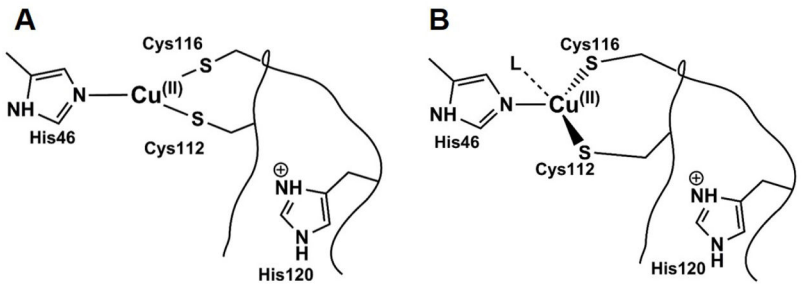

Fig. 6.

Schematic representation of the proposed identity of different I_x in the Cu_A variants. Two mononuclear I_x with 3-coordinate $Cu(Cys)_2(His)$ ligation for I_{x1s}(A), and as $Cu(Cys)_2(His)L$ (L= weak axial ligand) complex in distorted tetrahedral geometry for I_{x2s} (B) are proposed. Absolute residue numbering has not been experimentally assigned.

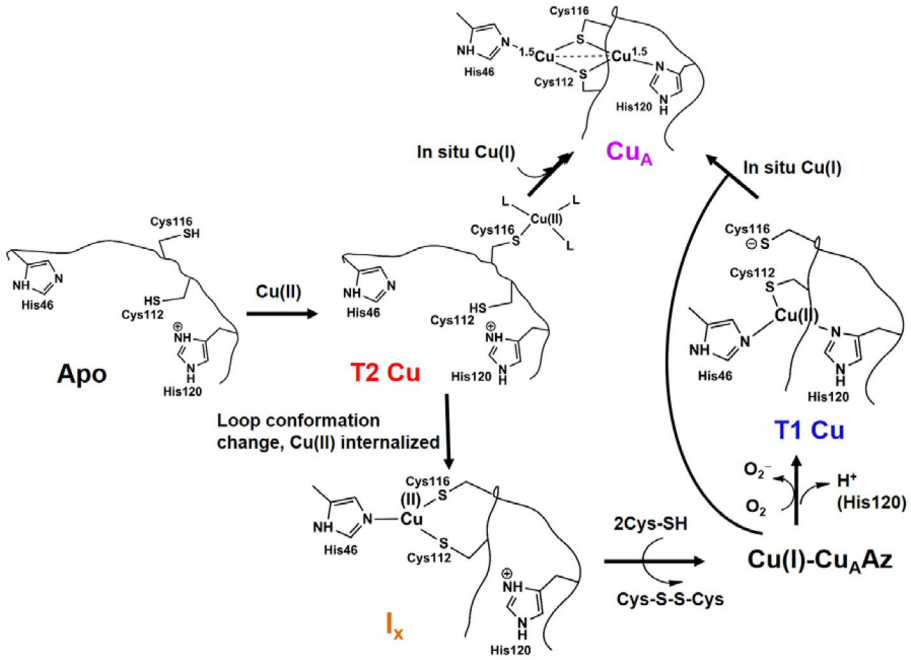

Scheme 1.

Proposed mechanism of Cu_A formation in Glu114XCu_AAz variants. Identity of the residues in the intermediates, and the protonation state of His120 have not been experimentally verified for the variants, and are proposed from what is known about Cu_AAz.

Table 1

Kinetic models used to fit the stopped-flow data shown in Fig. 2. Rate constants obtained from global analysis using Specfit are shown.

CuA Variant	Kinetic Model	Rate Constants
Glu114GlyCu_AAz		k_1 = 11.28 ± 0.35 s^{-1}
		k_2 = 1.95 ± 0.03 s^{-1}
		k_3 = (0.78 ± 0.04) × 10^{-3} s^{-1}
Glu114AlaCu_AAz	CuSO4 → T2 Cu T2 Cu → I_x I_x → T1 Cu	k_1 = 13.52 ± 0.52 s^{-1}
		k_2 = 0.46 ± 0.01 s^{-1}
		k_3 = (1.75 ± 0.05) × 10^{-3} s^{-1}
Glu114LeuCu_AAz		k_1 = 13.12 ± 0.98 s^{-1}
		k_2 = 0.34 ± 0.01 s^{-1}
		k_3 = (1.31 ± 0.05) × 10^{-3} s^{-1}
Glu114GlnCu_AAz		k_1 = 9.36 ± 0.66 s^{-1}
		k_2 = 0.31 ± 0.01 s^{-1}
		k_3 = (2.37 ± 0.06) × 10^{-3} s^{-1}

Table 2

EPR parameters extracted from simulation of the early time points EPR spectra shown in Fig. 4.

CuA Variant	Parameters				Populations[a]	
		I_{x1}	I_{x2}	Time	I_{x1}	I_{x2}
Glu114GlyCuAAz	g_x	2.034	2.027	50 s	38%	46%
	g_y	2.044	2.020			
	g_z	2.152	2.185			
	$\|A_x\|\times10^{-4}$ cm^{-1}	10	23			
	$\|A_y\|\times10^{-4}$ cm^{-1}	6	22			
	$\|A_z\|\times10^{-4}$ cm^{-1}	101	90			
Glu114GlnCuAAz	g_x	2.011	1.991	50 s	68%	18%
	g_y	2.035	2.092			
	g_z	2.151	2.249			
	$\|A_x\|\times10^{-4}$ cm^{-1}	20	8			
	$\|A_y\|\times10^{-4}$ cm^{-1}	14	41			
	$\|A_z\|\times10^{-4}$ cm^{-1}	82	133			
CuAAz[59]	g_x		2.007			
	g_y		2.056			
	g_z		2.234			
	$\|A_x\|\times10^{-4}$ cm^{-1}		9			
	$\|A_y\|\times10^{-4}$ cm^{-1}		0.3			
	$\|A_z\|\times10^{-4}$ cm^{-1}		115			
Tt CuA[56]	g_x	2.013				
	g_y	2.052				
	g_z	2.134				
	$\|A_x\|\times10^{-4}$ cm^{-1}	16				
	$\|A_y\|\times10^{-4}$ cm^{-1}	16				
	$\|A_z\|\times10^{-4}$ cm^{-1}	109				

[a] Only I_X present in the earliest time points are shown. See Table S2 for time-dependent populations of various species and their EPR parameters. Based on higher g_Z of Cu_A Az, the I_X can be categorized as I_{X2s} in the variants.

Table 3

Parameters extracted from fitting of the EXAFS data of I_X.

Sample/Fit	F	Cu-S (Cys)			Cu-N (His)			Cu-Cu[a]			E_0
		N	R(Å)	DW(Å^2)	N	R(Å^2)	DW(Å)	N	R(Å)	DW(Å^2)	
Glu114GlyCuAAz	0.53	2	2.17	0.016	1	1.97	0.02	0.15	2.412	0.0035	−0.76
Glu114GlnCuAAz	0.60	2	2.20	0.012	1	1.93	0.005	0.1	2.340	0.005	1.52

[a]Small amounts of the binuclear Cu_A forms present at the earliest time point samples.